UNIVERSITÀ DEGLI STUDI DI PADOVA

Dipartimento di Fisica e Astronomia "Galileo Galilei"

Corso di Laurea Triennale in Fisica

Tesi di Laurea

Realisation of light traps for a new generation of photodetectors based on wavelength shifting materials and silicon photomultipliers

Realizzazione di trappole di luce per una nuova generazione di fotorivelatori basati su materiali wavelength shifting e fotomoltiplicatori al silicio

Relatore

Prof. Mosè Mariotti

Laureanda

Veronica Marchiori

Anno Accademico 2023/2024

Contents

Abstract

When detecting unfocused photons in the UV bands, the "Light Traps" are an interesting alternative to large and inconvenient phototubes. The idea is to couple solid-state silicon light sensors with Wavelength Shifting Materials (WLS), used as light collectors. Such association enables increased performances in the light detection process, also providing a more cost-efficient solution in certain physics and astrophysics applications.
In this thesis we will review the main characteristics of this new kind of light traps, designed in single and double shift configurations of the WLS's and, based on some measures, we will assess the efficiency of two experimental double-shift light traps assembled with different WLS materials. Our results confirm the important advantages in the use of WLS, such as the shift of the incident UV light into the visible range and the significant "geometrical compression" effect of the incident light on the sensor surface. It is also confirmed that these systems are still characterised by a rather low efficiency.

Translation

Nella rilevazione di fotoni non focalizzati nelle bande UV, le "trappole di luce" costituiscono un'alterniva interessante all'impiego di grossi e scomodi fototubi. L'idea è di accoppiare sensori di luce allo stato solido con materiali (WLS), in grado di modificare le lunghezze d'onda della luce incidente, utilizzati come collettori di luce. Tale accoppiamento consente di incrementare le prestazioni del processo di rilevazione della luce, nello stesso tempo fornendo una soluzione meno costosa in alcune applicazioni nel campo della fisica e dell'astrofisica.
In questa tesi saranno esaminate le caratteristiche principali di questo nuovo tipo di trappole di luce nelle due configurazioni a singolo e doppio shift dei WLS e, sulla base di alcune misure, verrà valutata l'efficienza di due trappole di luce sperimentali in doppio shift con differenti materiali WLS.
I nostri risultati confermano gli importanti vantaggi nell'uso dei WLS, quali lo shift della luce UV incidente nel campo del visibile e il significativo effetto di "compressione geometrica" della luce incidente sulla superficie del sensore. Viene altresì confermato come questi sistemi siano caratterizzati da un'efficienza ancora piuttosto bassa.

Introduction

In particle physics and astrophysics, detection of light is a fundamental need for investigating many physics phenomena and, in the course of the years, several techniques have been developed to this purpose. Often, rather than a continuous flux of photons, fast light pulses, even formed by single or few compacted incoming photons, have to be detected and measured. To this purpose, fast and sensitive photodetectors are needed. The capability to detect the single photons over the electronic noise, require a process of strong electron multiplication after the initial photo electron extraction.

The so called "light traps" are devices in general designed for capturing and keeping the light within the trap itself and for collecting and conveying photons to the surface of a light sensor that usually is a vacuum tube known as Photo Multiplier (PM). More recent solid-state photodetectors, as the so called Silicon Photomultipliers (SiPM), are formed by an array of Geiger mode avalanche photodiodes cells.
A further improvement is the utilization of "Wavelength Shifting Materials" (WLS). The fundamental property of such materials is the ability to absorb light at one wavelength and to re-emit isotropically the light at longer wavelengths. As a result, by collecting and conveying the incoming light through a suitably shaped WLS underlayer, UV or blue photons can be shifted to lower frequencies and especially conveyed and concentrated on the small surface of a SiPM.

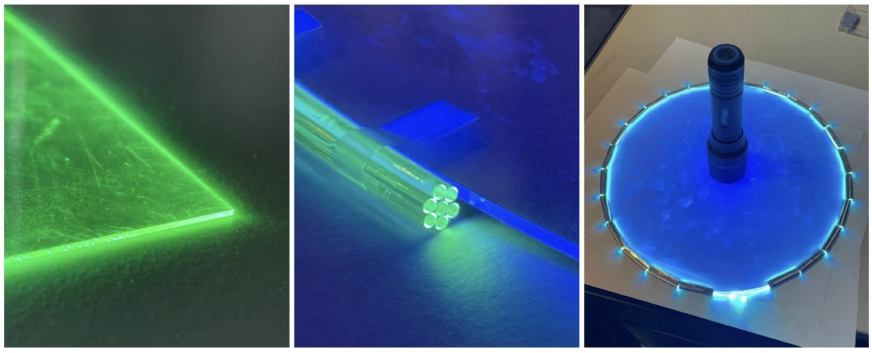

Figure 1

The purpose of this thesis is to measure and assess the main performances of an innovative type of light trap fitted with WLS materials and solid-state Silicon Photomultipliers. To this extent we will go through the following steps:

1. Review of the basic operation principia of SiPMs and WLS materials;
2. Key characteristics of SiPMs and basic criteria of photon counting;
3. Concepts of light trapping in single and double shift layout, effects of geometrical compression, and relevant effects on the light pulse waveform;
4. Efficiency of light traps calculation, based on experimental measures.

Chapter 1

A new concept of photodetectors

1.1 Photomultipliers

A Photomultiplier (PM) is a device or system designed to detect and amplify the electronic signals coming from photoelectrons extracted by photons received from a light source.

The amplification process is based on the photoelectric effect and this phenomenon, also known as "secondary emission", is typical of certain materials. When the surface of the dynodes is struck by an electron, the material is induced to release a number of new electrons as an effect of the partial transfer of the incoming electron energy to the material itself.

The most common type of PM is the "Photomultiplier Tube" (PMT), also called "Phototube". In general, PMTs are formed by a vacuum tube fitted with a photocathode and a series of dynodes located before the anode. Dynodes are small electrodes that work as photoelectron multipliers. The few electrons emitted by the cathode are accelerated towards the first dynode by a suitable electric field set into the PMT. By striking the surface of the dynode, each electron induces the emission of several new photoelectrons which, in turn, are again accelerated by the electric field and move to strike the second dynode, so generating more new photoelectrons.

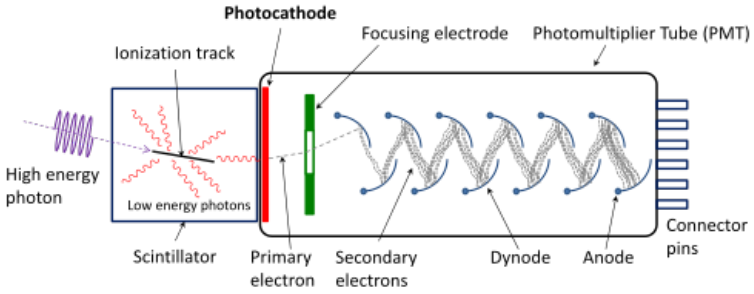

Figure 1.1: Scheme of a PMT [13].

Although PMTs are very useful to detect weak light signals, providing high sensitivity to single photons and a fast response time too, unfortunately they show some application disadvantages:

- Mechanical fragility of the vacuum tube,
- Limited photon detection efficiency (QE),
- Expensive,
- High voltage of the electric field necessary to operate the PMT (1000 ÷ 1500V).

Much better performances can be obtained with other kind of detectors, more recently developed. Among these, the "Silicon Photomultiplier" (SiPM) is a highly sensitive solid-state PM formed by an array of "Avalanche Photodiodes" (APD) set to work in the so called "Geiger-mode", i.e. enabling the detection of single incoming photons.

A suitable number of APDs, each of them constituting a "pixel" or "cell", is assembled in arrays where all APDs are connected in parallel and each of them is also fitted with a quenching resistor in series. The pixel's size can vary typically between 10 and 100 micrometers.

The APD P-N junctions are operated with high reverse bias, i.e. the APD works as a diode close to its reverse breakdown voltage. In this way the charge carriers in the semiconductor, i.e. electrons or holes generated by the photoelectric effect, are multiplied by the induction of an avalanche breakdown, so providing a significant amplification effect.

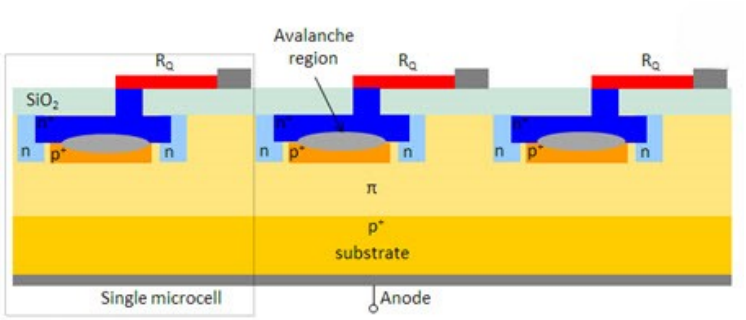

Figure 1.2: Schematic of a SiPM [11].

More in detail a SiPMs works as follows:

- **Absorption of photons:** as a photon enters into the APD, it interacts with the silicon material and excites the electrons of the valence band to the conduction band, creating electron-hole pairs. These pairs are generated in the so-called depletion area, a neutral charge region located near the P-N junction;
- **Separation of the charge carriers:** the electron-hole pairs are subjected to the internal electric field that inversely polarize the ADP (reverse bias). This field can separate the pairs. In this way, electrons move toward the N-type region and holes move toward the P-type region;
- **Avalanche Multiplication:** the internal electric field has also the effect of accelerating the photo-generated carriers well above the ionization energy limit of the silicon, so allowing electrons to be knocked out of the atoms. In other terms, when the electric field is strong enough, the carriers are accelerated to energy high enough to kick other carriers out, i.e. triggering the generation of new carriers. This process results in an avalanche of charge multiplication, also called "avalanche breakdown", significantly amplifying the initial charge generated by the incoming photon and providing a detectable electric signal at the APD pins;
- **Geiger-mode:** the APDs forming the SiPM can also be designed for safely working above the reverse-bias breakdown voltage, i.e. above the minimum reverse voltage that makes the diode appreciably conducting in reverse. In these conditions, a high speed of the avalanche breakdown is induced and this allows an effective detection of single photons providing as output, short duration trigger pulses which can be counted as it would be done in a Geiger counter. APDs working in this way are indicated as Geiger-mode Avalanche Photo Diodes (GAPD);

- **Quenching and restart of the GAPD:** the avalanche breakdown is a self-sustaining phenomenon that needs to be terminated at a certain moment in time, so providing the reset of the GADP and restoring the Geiger-mode for a new detection process. To this purpose, a quenching circuit is necessary to cut-off the current flow generated by the multiplication process. The simplest way for quenching the GAPD is connecting a sufficiently large resistor in series to the photodiode. This method provides a fast quenching of the avalanche current even if, in the meantime, may result in a quite long reset time due to a capacitive depletion effect of the GAPD (RC-circuit delay).

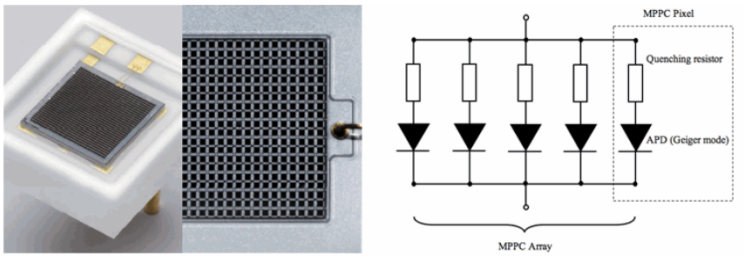

Figure 1.3: Schematic of a SiPM as array of GADPs [11]

In summary, a GADP operated above the reverse-bias breakdown voltage, provides an output signal formed by pulses, each one corresponding to the detection of a single photons. Now, considering a whole array of GADPs, the amplitude of the pulses is proportional to the number of photons detected within a given time interval by the array. Therefore, by counting the number of pulses given by the SiPM in a certain time, it's possible to determinate the initial number of the incident photons.
Since SiPMs are formed by arrays of many GADPs, it's important that the numbers of photons which hit the arrays is much less than the number of pixels. Indeed, if two or more photons would strike the same cell, this would anyway produce a single signal seen as corresponding to one single photon.

There are some important parameters that characterize the performances of PMs (PMT or SiPM). For tracing back to the information conveyed by the single incident photon, it's important to know the PMT amplification factor or "Gain". The gain expresses how much the PMT is able to increase the initial signal enabling the effective processing by the downstream electronic circuits. Another parameter is the "Quantum Efficiency" (QE), indicating how much effectively the PMT converts incident photons into photoelectrons. QE is expressed by the ratio between the number of photoelectrons emitted by the PMT dynodes and the number of incident photons.

The most important key characteristic of a PM is the Photon Detection Efficiency (PDE). The PDE is the probability that, in response to an incident photon, a photoelectron is generated inducing an avalanche. This probability is expressed by the following formula:

$$PDE = QE \cdot \epsilon_f \cdot P_t \cdot P_a \tag{1.1}$$

where $Q.E.$ is the quantum efficiency, ϵ_f is a geometrical factor, also called "fill factor", depending on dimensions and shape of the PM, P_t is the probability that a photon is absorbed by the depletion region and P_a is the probability for a electron-hole pair to generate an avalanche.

Compared to the PMTs, SiPMs show some application advantages:

- More compact, robust and light weight;
- Operate with low voltage ($\sim 20 - 100V$);
- Provide higher PDE;
- Higher sensitivity;

- SiPMs are much cheaper as a "single unit" than PMTs.

Instead, SiPMs show higher noise than PMTs resulting from a certain sensivity to the temperature. Finally, we have to note that, SiPM surface do not usually exceed one square centimetres and therefore, assembling large-surface photodetectors by using many SiPMs in arrays, may result in much higher costs than PMTs. Therefore, for large detectors, PMTs are still the preferred solution.

1.2 Wavelength-shifting materials

The Wavelength Shifters (WLS) are materials (in general aromatic hydrocarbons like benzene and triphenyl) that, upon absorbing high-frequency photons, re-emit isotropically one or more lower-frequency photons into the material itself. This process is relatively fast with an exponential decay time of few nanoseconds.

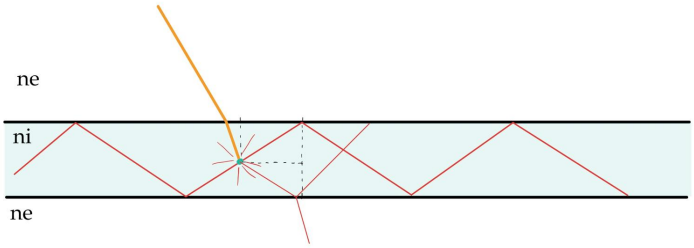

Figure 1.4: Schematic of WLS photon isotropic diffusion.

As a consequence of this property, a conveniently shaped WLS could be used as "collector" of the incoming photons, like shown in Fig. 1.4 where a two parallel surfaces geometry has been considered. In order to benefit from the isotropic diffusion of the shifted photons, it's beneficial that they do not "escape" from the "entrance window", remaining "trapped" inside the WLS material. In this way the shifted photons could be detected through a PM conveniently positioned on a lateral surface of the WLS. As we will see later on, a "trapping efficiency" can be calculated as a function of the refractive indexes of both WLS and external medium.

In addition, two different kinds of WLS properly shaped and coupled, would also provide:

- a double wavelength shift of the incoming light, increasing the frequency shift towards the visible range;
- an important effect of light concentration due to the geometrical compression, from the larger collecting surface of the first WLS to the smaller exit surface of the second WLS located right in front of the SiPM pixels.

The particular property of WLS materials suggested the possibility of effectively using PMTs for detecting UV or blue photons by shifting them in the visible band, so enabling a better operation of the PMT. Additionally, a conveniently shaped WLS material allows covering relatively larger light collection areas and this would evidently result in a reduction of the costs associated with a standard PMT application.

If from one hand, WLS materials have found applications in the industries of photovoltaic cells, optical fibres and LED lamps, from the other one, this technology is also of big interest in important physics international experiments aimed to detect the Cherekov light produced by charged particles moving at high speed in a dielectric medium. As an example, experiments like "IceCube" in the Antarctica and "Super-Kamiokande" in Japan, have been aimed to detect neutrinos from cosmic rays. The "MAGIC" telescope in the Canarian Islands and the planned new SWGO telescope in South America are instead aimed to detecting extra-terrestrial Gamma-rays.
High energy particles entering the earth atmosphere, generate an electromagnetic cascade of

positrons and electrons, often referred to as "shower". This shower of particles can be detected by taking advantage of the well-known Cherenkov effect. In particular, the detection of the Cherenkov radiation produced into water tanks fitted with PMTs located on the tank bottom, has been proven to be a very good and effective method for detecting the shower of high energy particles.

In conclusion coupling PMT and WLS materials might be a further step for upgrading and improving high-energy particle detection processes and, exactly to this extent at IceCube observatory, the Wavelength-shifting Optical Module (WOM) has been developed as new generation of PD.

1.3 Application of SiPMs together with WLS material

The design of new kinds of light traps, based on the earlier mentioned features of coupled WLS materials and SiPMs, is a promising application for detecting UV photons leading to a new valid alternative to the standard PMTs applications.

To this purpose, within the Physics Dept. of the University of Padua, we have realized an experimental light trap based on the a.m. concepts, aimed to simulating the detection of unfocused photons and measuring the main features provided by the system. Basically, the light trap set-up is as follows:

- As light collectors, we have tested two kinds of WLS underlayers, one shaped as a square with 15 cm side dimension and the other one shaped as a disk with 10 cm radius. For the double-shift layout configuration, as first shifter a WLS disk was used, alternatively surrounded with two types of WLS fibers. The WLS materials adopted were from Eljen Technology (types EJ-282 and EJ-286 for the first shifter) and Kuraray (types YS-2 and YS-6 for the fibers).

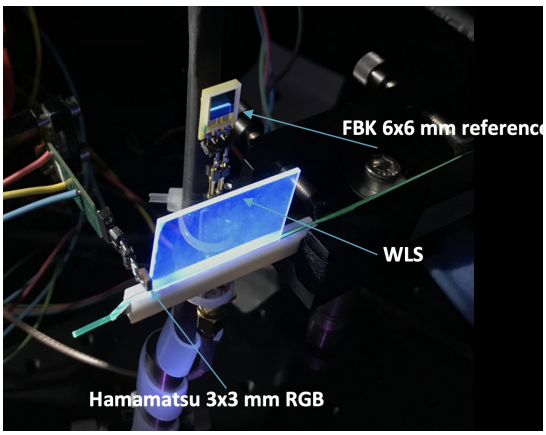

Figure 1.5: Light trap with single-shift layout, the SiPM located on a side border enables the collection of light.

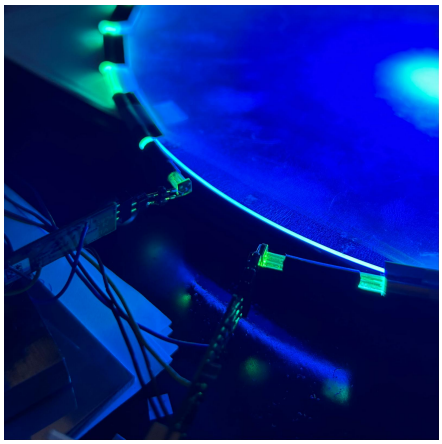

Figure 1.6: Light trap with double-shift layout, the two SiPMs are positioned at the fibre ends to collect the light.

- The SiPM adopted was a commercial photodetector Hamamatsu 3 x 3 mm^2 (s14160-3050HS serie) with the following features:

TYPE. no.	number of channels	photosensitive area/channel	pixel pitch	number of pixels	geometrical fill factor
S14160-3050HS	1	3 x 3 mm^2	50 μm	3531	74%

Table 1.1: Structure of the S14160-30250HS SiPM used for measurements

Parameter	value for S14160-3050HS
Spectral range response λ	270 to 900 nm
PDE at 450 nm (peak sensitivity)	50%
Breakdown voltage V_{br}	38 V
Recommended operating voltage	V_{br}+2.7V
Cross talk probability	$\sim$ 7%
Gain	2.5 x 10^4

Table 1.2: Electrical and optical characteristics of the S14160-30250HS Sipm at $T = 25°$ and $V_{\text{over}} = 2.7V$

- As light source we have used a PicoQuant Laser able to generate light beams in the UV energy range. In particular, the light beam has been collimated for providing a picosecond-pulsed light source (LDH-P-C-375). The laser pulse parameters and power are summarized in the following table:

Parameter	value for LDH-P-C-375
Wavelength	375($\pm$ 5) nm
Pulse (FWHM)[1]	<90 ps
Max repetition rate	40 MHz
High avg. power[2]	2.0 mW
Low avg. power[3]	0.6 mW

- For the data acquisition, the electric signals made available by the SiPM were processed through an oscilloscope WavePro 254HD (2.5 GHz, 20 GS/s, 4ch, 100 Mpts/Ch High Definition Oscilloscope).

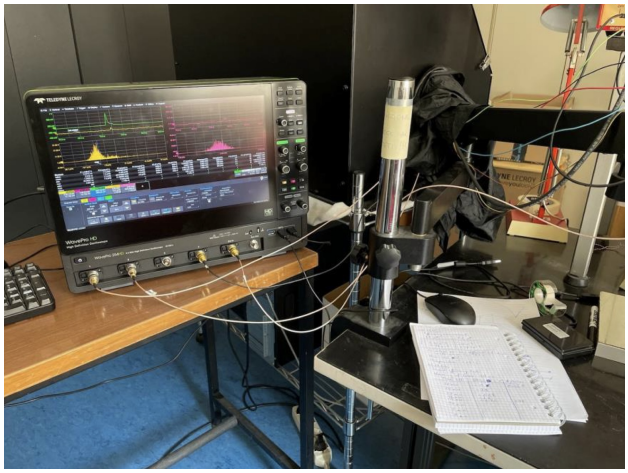

Figure 1.7: External set up for measurements.

[1]Shortest pulse width at min intensity setting above laser threshold.
[2]Average optical power at max repetition rate and max intensity setting.
[3]Average optical power at max repetition rate and min intensity setting above laser threshold.

Chapter 2

Photon counting with SiPMs

As previously seen, SiPMs could be a valid alternative to PMTs. For this reason, we will characterize them by the most important features and focus the methodology for measuring a flux of incoming photons.

2.1 Characteristics of Silicon Photomultipliers

Besides the earlier mentioned Quantum Efficiency (QE) and Photon Detection Efficiency (PDE), there are some other parameters that characterize every silicon photomultiplier.

1. **Gain:** This characteristic indicates the internal amplification factor of the SiPM and is expressed by the average number of charge carriers forming the avalanche in Geiger mode. The gain depends on the bias voltage and the SiPM working temperature. Actually, during SiPM operation, some thermal-electrons can be generated and they could induce "unwanted" secondary avalanches that would overlap the initial breakdown avalanche generated by the incoming photon.
2. **Noise:** Each electronic amplification chain produces undesired internal electric noise that add up to the measured signal causing its degradation. For a SiPM we can identify three causes of noise:
   - **a. Thermal noise:** This is due to the thermal vibrations of electrons within the SiPM material caused by internal changes in the charge distribution. The macroscopic result is a temperature-dependent noise increase.
   - **b. Dark current noise:** Even in absence of any incident light, as an effect of the temperature, the generation of some spurious events may still be possible. More in detail, the thermal electrons generated inside the SiPM, depending on their energy level, can even trigger electron-hole pairs which, in turn, may be able to initiate an avalanche without any actual incident signal. This occurrence can be evident especially in low-light conditions.
   - **c. Aferpulsing:** The charge carriers in the depletion region can remain trapped by material impurities at intermediate energy levels during the avalanche process and, as a result, they can be released with a certain delay. This means that a delayed avalanche can be generated, overlapping the initial one, i.e. creating another source of noise. The probability that an afterpulsing effect occur, increases with the amount of charge flowing through the photodiode during the Geiger discharge. Thus, the afterpulsing probability rises with the increase of the bias voltage.

3. **Cross Talk:** Since APSs are assembled in arrays, the avalanche photoelectrons generated by a GAPD may also fall within the detection range of other neighbouring pixels, triggering one or more secondary avalanches. Referring to Fig. 2.1, these secondary discharges are nearly simultaneous with the primary one (Prompt Crosstalk) when the photoelectron can directly reach the avalanche region of an adjacent cell. Instead, the secondary discharges are delayed by some nanoseconds (Delayed Crosstalk) when the photoelectron just trigger charge carriers nearby the avalanche region. Finally, if the photoelectron is dispersed in the substrate there is No Crosstalk.

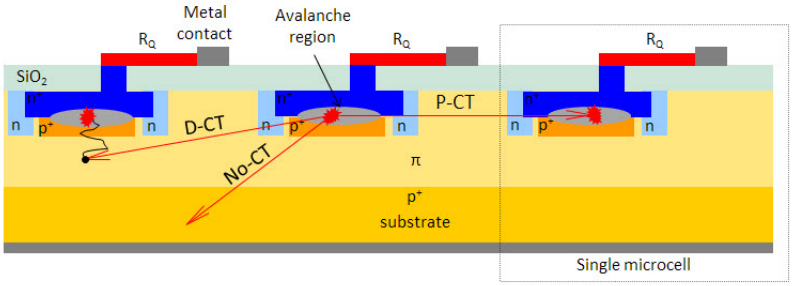

Figure 2.1: Mechanisms of prompt crosstalk (P-CT), delayed crosstalk (D-TC) and no crosstalk (No-CT) [12]

Although the Crosstalk is not a thermal phenomenon, it can actually be considered an additional source of noise. The Crosstalk influencing factors are: the pixel size, the SiPM assembly structure and the difference between the bias voltage and the breakdown voltage.

4. **Signal-to-noise ratio (SNR):** The intensity of the input signal versus the noise generated by the device is an important feature. A higher SNR results in higher quality of the measures. To this purpose, by comparing different supply voltages, it is possible to identify those optimal operational conditions providing a better SNR.

5. **Excess Noise Factor (F):** In simple words, the Excess Nois Factor F can be intended as a sort of "gain noise". All avalanche photodiodes generate a kind of "excess noise" due to the statistical nature of the avalanche process. More precisely, the distribution of photoelectrons in the avalanche is not uniform and generates current fluctuations depending on the material, the impact ionization currents and the energy bandwidth of the incoming photons. Actually, the Excess Nois Factor F is a multiplicative correction, representing the contribution associated to the current fluctuations in the multiplication process. Therefore, F is equal to 1 in the ideal noiseless photodiode (PIN) where there is no multiplication effect, and is above 1 for all PM, SiPMs included, in real conditions.

2.2 Photon flux measurement

The key measures with SiPMs are the number of the incoming photons and the number of generated photoelectrons. Supposing we know the SiPM efficiency PDE and the number of photoelectrons generated, the number of incoming photons is given by:

$$\#ph = \frac{\#phe}{PDE}$$

where $\#ph$ are the incoming photons, $\#phe$ the produced photoelectrons by the photons and PDE is the photon detection efficiency.
The distribution of the generated photoelectrons depends on several factors including the characteristics of the light source, the sensitivity of the photosensor itself, and the duration of the measurement. The whole photoelectrons distribution, as visualized through an oscilloscope (Fig. 2.2), recalls the Poisson curve that is therefore a good statistic tool for counting the photoelectrons.

The Poisson distribution is given by:

$$P(n, \mu) = \frac{\mu^n}{n!} e^{-\mu} \tag{2.1}$$

where $P(n, \mu)$ is the probability that a number n of photoelectrons are detected in a given time and μ is the average number of photoelectrons in the same time interval.
Actually, there is an irreducible statistic error coming from the Poisson distribution that is expressed by the standard deviation $\sigma = \sqrt{\mu}$. This error, overlaps the other "noises" that influence the measures.

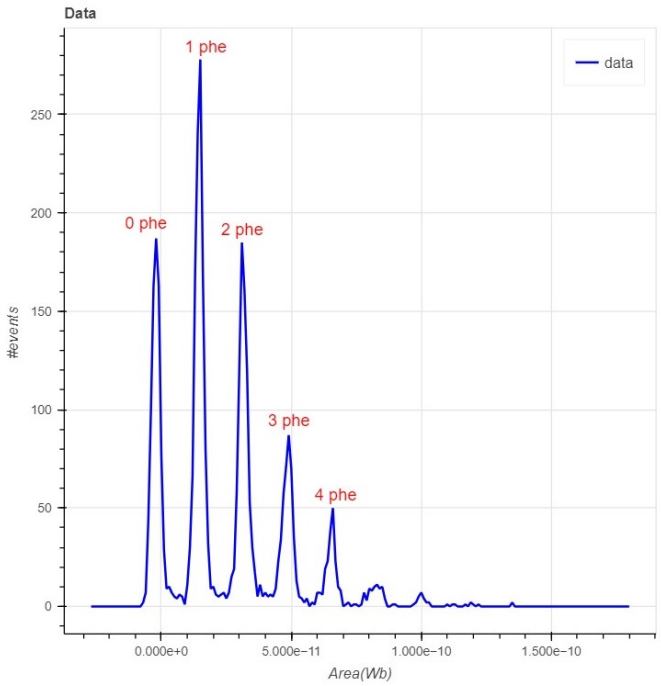

Figure 2.2: Example of a distribution of peak height of the signal obtained at 42 V with laser-generated UV wavelength and 50Ω closing circuit resistor. This Poisson distribution has $\mu \sim 1$ phe.

Referring to Fig. 2.2, the Poisson distribution of the signal detected recalls a series of Gaussian functions. Each peak represents the probability that a given number of photoelectrons is detected and is expressed in number of events. Therefore, the first peak population represents the probability for 0 photoelectrons, the second one for 1 photoelectron, the third one for 2 photoelectrons, and so forth.

As variable for the horizontal axis, instead of numerating the average number of incoming photons (n), it is more convenient to trace back to their total charge. Indeed, dimensionally we have:

$$C = A \cdot s = \frac{V \cdot s}{\Omega} = \frac{Wb}{\Omega} \qquad V \cdot s = Wb \tag{2.2}$$

As a result, by measuring the voltage on the resistor closing the SiPM overall amplification chain in a fixed time interval, we can deduct the total integrated charge of the photoelectrons. Indeed, we have to consider that more photons are detected at the same time because they hit simultaneously different cells and therefore, the resulting waveform is a cumulative curve representing a sum of signals detected by each fired pixel.

In addition, when using a WLS layer, due to the characteristic of the material, not all photons reach the SiPM pixels at the same time and therefore the production of photoelectrons is in some way delayed. Therefore, measuring an integrated charge allows not to lose any information on the incident light.

For correctly executing the above measures, it is necessary establishing the influence (level) of Crosstalk, as this is a steady effect present in all measures. In other terms, we have to calibrate the measuring process on the actual Crosstalk and this can be made by identifying the "Single Photoelectron Distribution" (SPED), also called "dark count".

In absence of light, we can expect that sporadic photons hit the cells and quite few photoelectrons are generated. In this situation (light source off), by triggering the oscilloscope on the photodiode, instead of on the light source, the detection of single photoelectron is possible. The relevant distribution (Fig. 2.3) shows an evident peak corresponding to the SPED and few other small peaks caused by the Crosstalk events.

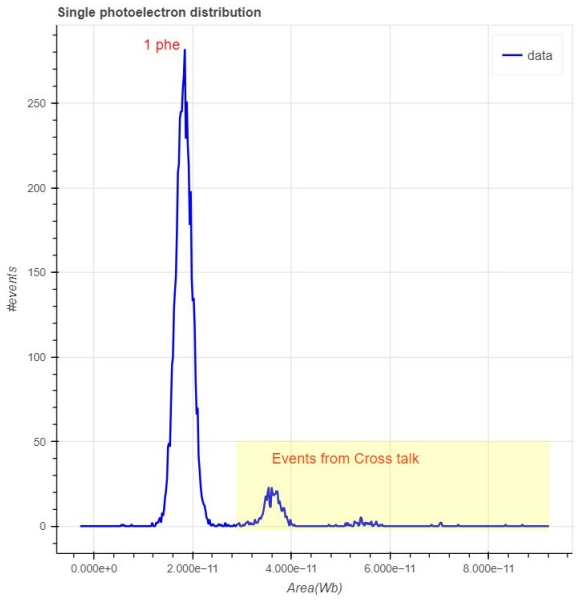

Figure 2.3: Example of the single photoelectron distribution obtenied at 42 V

More in detail, for evidencing the SPED, the triggering level should be higher than the electronic noise voltage, but lower than that one corresponding to observing one photoelectron.
As we will see later on, besides assessing the magnitude of the Crosstalk effect, the SPED calibration enables also to estimate the gain of the system at that particular bias voltage used.

2.2.1 Measurement of a weak photon flux

From the Poisson distribution we can deduct the average number of photoelectrons μ in a given time frame.
However, the situation is rather different whether the flux of incoming photons is strong or weak. Actually, with a strong flux is difficult or even impossible distinguishing the peaks corresponding to the generated photoelectron. On the contrary, with a weak flux the peaks are well shaped and identifiable.

Let's consider for the moment just the case of a weak photon flux (as an indication, less than 10 photons). Considering a generic Poisson distribution like that shown in fig 2.2, the probability to observe zero photoelectrons $P(0)$ is:

$$P(0) = \frac{\#\text{events of the 0 peak}}{\#\text{total events}} \tag{2.3}$$

Therefore, from the equation 2.1, we can derive the average number of photoelectrons μ, as:

$$\mu = -ln(P(0)) \tag{2.4}$$

We will see later on how to calculate μ with a strong photon flux.

2.2.2 Measurement of the gain and the crosstalk

As previously seen, Gain and Crosstalk are two important parameters for assessing the quality of the measures. For a specific bias voltage, it is highly desirable that the gain remain stable in a certain range as this indicates that the SiPM is not affected by external disturbances as temperature and saturation effects. Likewise, it is useful to evaluate the Crosstalk expressing it as a share of $P(n, \mu)$.

The Gain has to be intended not only the internal amplification effect of the SiPM, but the total effect of the whole amplification chain. This is influenced by the working temperature, the bias voltage and also depends on the time integration gate.
There are three methods for calculating the Gain:

1. By using the Poisson distribution and knowing the average number of photoelectrons μ, the Gain can be expressed as:
$$G = \frac{\bar{A}}{\mu} \tag{2.5}$$
where $\bar{A}$ is the average amplitude of the signal. Since the signal amplitude distribution may be shifted from the zero, it may be necessary to correct $\bar{A}$ by subtracting the average amplitude of the distribution pedestal $\bar{A}_{ped}$ and therefore, the previous equation would be corrected in:
$$G = \frac{\bar{A} - \bar{A}_{ped}}{\mu}$$

2. Recalling the SPED meaning, this distribution represents the single photon detection while the other following events identify the Crosstalk. In this case the Gain corresponds to the average amplitude of the distribution:
$$G = \bar{A}_{SPED} \tag{2.6}$$
If the detector would be an ideal one without any type of noise, the SPED would be represented by one single peak and therefore the Gain would correspond to the average value of the Gaussian that fits the first peak. Since the SPED is affected by the Crosstalk, the true average amplitude distribution may result affected by the integration gate chosen for the measures. Therefore, while a too short integration gate would cut some events, a larger one would also collect unwanted afterpulsing effects.

3. Considering now the case of a whole amplitude distribution where the Crosstalk is limited or even negligible, the Gain could also be evaluated as the distance between two consecutive peaks, i.e. as the difference between the average values of two consecutive Gaussian distributions ($\bar{x}_0$ and $\bar{x}_1$).
$$G = \bar{x}_1 - \bar{x}_0 \tag{2.7}$$
On the contrary, i.e. in presence of a significant Crosstalk, this method provides a certain Gain underestimation because it directly refers just to two single peaks of the distribution and in this way the crosstalk events would be disregarded.

In conclusion, the first method is the most practical and convenient to use.

Coming now to the Crosstalk, we saw that secondary avalanche breakdowns can be triggered in the adjacent cells upon detection of spurious photoelectrons. We also saw that Crosstalk emerges evident from the SPED distribution (fig. 2.3). As a result, having available the SPED, the probability of Crosstalk (P_{CT}) can be calculated as:
$$P_{CT} = \frac{1 - P_1}{P_1} \ \% \tag{2.8}$$

where the P_1 is probability for the first peak.
In the same way the relation 2.8 is connected with the number of events of each peak. So this equation can be transformed using the events:

$$P_1 = \frac{\#\text{event}_1}{\#\text{event}_{\text{tot}}} \qquad P_{CT} = \frac{\#\text{event}_{\text{tot}} - \#\text{event}_1}{\#\text{event}_1}\ \% \tag{2.9}$$

where $\#\text{event}_{\text{tot}}$ is the total number of events and $\#\text{event}_1$ is the number of events of the first peak.

Both Gain and Crosstalk depend on bias voltage and temperature. Therefore, our measures were carried out by keeping the system temperature stable in the range 26,6-26,9°C while Gain and Crosstalk were calculated as a function of the bias voltage in the range 40-43V.

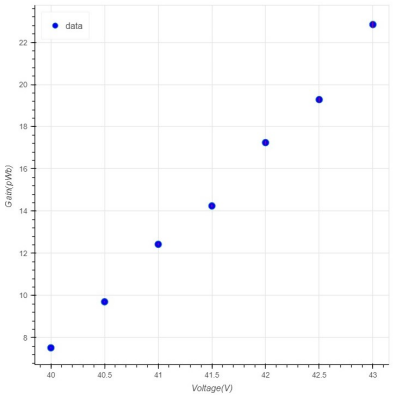

Figure 2.4: Gain measurement versus bias voltage (Gain calculated with method #1)

Voltage (V)	Gain (pWb)
40	$7,52 \pm 0,03$
40,5	$9,704 \pm 0,03$
41	$12,43 \pm 0,05$
41,5	$14,246 \pm 0,06$
42	$17,25 \pm 0,09$
42,5	$19,28 \pm 0,10$
43	$22,84 \pm 0,14$

Table 2.1: Results of data analysis

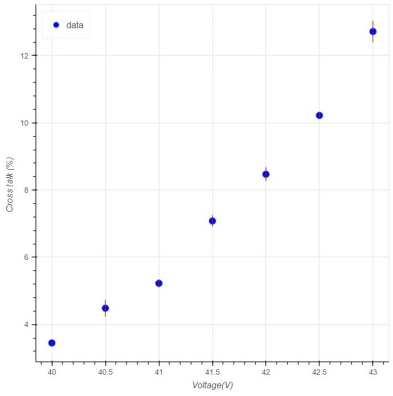

Figure 2.5: Crosstalk measurement versus bias voltage

Voltage (V)	$P_{CT}(\%)$
40	$3,45 \pm 0,08$
40,5	$4,48 \pm 0,25$
41	$5,23 \pm 0,13$
41,5	$7,08 \pm 0,17$
42	$8,47 \pm 0,21$
42,5	$10,22 \pm 0,10$
43	$12,72 \pm 0,32$

Table 2.2: Results of data analysis

2.2.3 Measurements of a strong photon flux

With a strong flux of photons, it is difficult or even impossible to identify and isolate the peaks in the Poisson distribution and therefore determining the average number of photoelectrons as we have done with the previous method. In such conditions μ can be calculated through the statistic characteristics of the intensity distribution.

In an ideal noiseless detector, when the excess noise factor is close to 1, the Poisson distribution is perfectly shaped and therefore, recalling the equation 2.5 we have:

$$\bar{A} = G \cdot \mu \qquad \sigma_A = G \cdot \sqrt{\mu}$$

where G is the gain, $\bar{A}$ is the average amplitude and σ_A is the standard deviation.
Therefore, the average number of photoelectrons is:

$$\mu = \left(\frac{\bar{A}}{\sigma_A}\right)^2 \tag{2.10}$$

The Poisson curve is also characterized by its pedestal that represents a certain number of minor events. In order to take these events into account, the average amplitude of the pedestal $\bar{A}_{ped}$ and the relevant standard deviation σ_{ped}, have to be considered and therefore the previous equation can be corrected in:

$$\mu = \frac{\left(\bar{A} - \bar{A}_{ped}\right)^2}{\sigma_A^2 - \sigma_{ped}^2} \tag{2.11}$$

This relation is a first approximation for calculating μ in presence of a strong flux of photons and is valid when the excess noise factor $F \sim 1$, i.e. only in presence of the pure statistical noise due to the Poisson distribution.
In a more general situation, there is always a real noise that exceeds the statistical fluctuations and therefore an actual excess noise factor $F > 1$ has to be considered.

Since F is a multiplicative factor, the actual average number of photoelectrons μ^* can be expressed by correcting the previous equation in:

$$\mu^* = \frac{\left(\bar{A} - \bar{A}_{ped}\right)^2}{\sigma_A^2 - \sigma_{ped}^2} \cdot F^2 \tag{2.12}$$

Assuming now that F is the same factor we would have in the case of a weak flux of photons, from eq. 2.4 results:

$$F^2 = -ln(P(0)) \cdot \frac{\sigma_A^2 - \sigma_{ped}^2}{(\bar{A} - \bar{A}_{ped})^2}$$

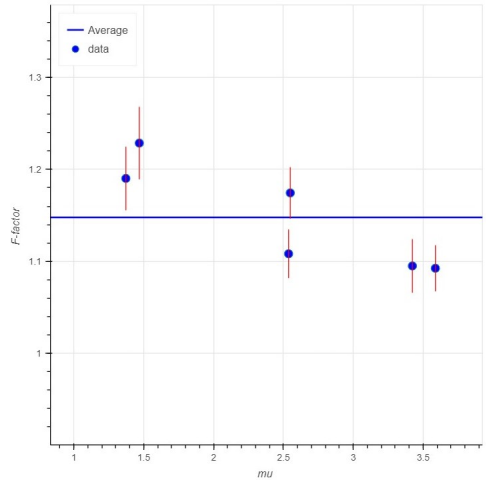

Figure 2.6: Plot of the F-factor respect to the average number of photoelectrons

μ^*	μ	F^2
$1,39 \pm 0,03$	$1,37 \pm 0,02$	$1,19 \pm 0,03$
$1,47 \pm 0,04$	$1,47 \pm 0,03$	$1,23 \pm 0,04$
$2,47 \pm 0,05$	$2,54 \pm 0,03$	$1,11 \pm 0,03$
$2,58 \pm 0,05$	$2,55 \pm 0,03$	$1,17 \pm 0,03$
$3,37 \pm 0,08$	$3,42 \pm 0,04$	$1,10 \pm 0,03$
$3,56 \pm 0,08$	$3,59 \pm 0,03$	$1,09 \pm 0,03$

Table 2.3: Results of data analysis (fixed parameters $V_{bias} = 42V$ and $T = 25,5°$)

The average value of F-factor calculated from the data is:

$$\bar{F}^2 = 1.15 \pm 0.05$$

2.2.4 Signal-to-noise ratio

As previously seen, the optimal working conditions can be identified by measuring the Signal to Noise Ratio (SNR) as a function of the bias voltage. Clearly, the higher is the input signal and the lower is the intrinsic noise of the device, the better the quality of the measures taken will be. Considering now the intensity distribution of a SiPM with an average amplitude $\bar{A}$ of the signal and a standard deviation σ_A, this ratio can be expressed as::

$$S/N = \frac{\bar{A}}{\sigma_A} \tag{2.13}$$

The bias voltage V_{bias} is the external parameter governing the multiplication effect and, in the meantime, the PDE and the noise in form of Crosstalk. As a consequence, the SNR is directly depending on the bias voltage.
We have carried out some measures aimed to identify a range of V_{bias}, where the SNR is sufficiently stable. In particular, $\bar{A}$ and σ_A have been measured directly on the oscilloscope by keeping constant the intensity of the laser source, while changing the bias voltage into a certain range.

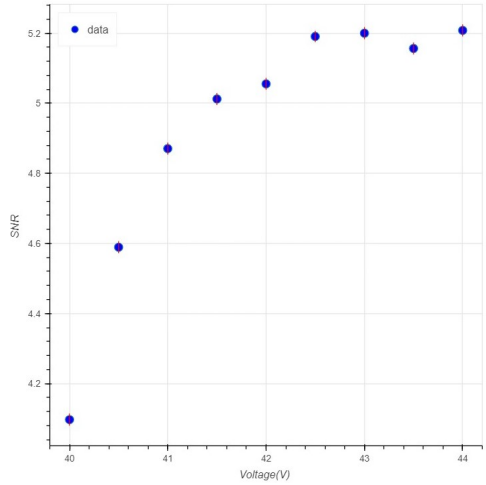

Figure 2.7: Plot of the SNR respect to bias voltage

Voltage (V)	SNR
40	$4,10 \pm 0,02$
40,5	$4,59 \pm 0,02$
41	$4,87 \pm 0,02$
41,5	$5,01 \pm 0,02$
42	$5,06 \pm 0,02$
42,5	$5,19 \pm 0,02$
43	$5,20 \pm 0,02$
43,5	$5,16 \pm 0,02$
44	$5,21 \pm 0,02$

Table 2.4: Results of data analysis (fixed parameter $T = 27°$)

The data acquired show that a "plateau" for SNR can be identified within $V_{bias} = 42,5 - 44,0V$. Therefore, a bias voltage in this range would maximize and stabilize the SNR. However, keeping into consideration that the bias voltage is also directly influencing the Crosstalk, in order to reduce a bit this effect, the most convenient bias voltage could be around 42V, i.e. at the plateau starting point. This is the reason why all measures in this work have been taken at this voltage.

Chapter 3

Wavelength-shifting light traps

The utilization of Wavelength Shifting materials as light collectors is actually beneficial for improving the light trap operation, basically for the following reasons:

- The WLS layer can be suitably shaped for optimizing the light collection process making sure that almost all light is conveyed to the PM;
- The shifted light isotropic dispersion enables finding the most convenient position for the PM;
- Shifting high energy photons to lower frequencies in the visible range, is beneficial for a better operation of the PM;
- Coupling two different WLS materials enables the maximum geometrical compression effect, so allowing the maximum concentration of the incoming light on the SiPM pixels.

The selection of proper WLS is clearly depending on the incoming light wavelength. For our purposes, as light source we considered only UV light and then, we identified materials suitable to provide shifts in the visible blue and green ranges.

3.1 Concepts of light traps

The selected WLSs are from two different manufactures: Eljen Technology for slab shaped layers and Kuraray for the fibres.
Within the Eljen Technology assortment, the following WLS were selected:

- **EJ-282**: is a green-emitting WLS plastic with a slightly shorter maximum emission wavelength making it suitable for use with blue-sensitive photomultiplier;
- **EJ-286**: is a blue-emitting WLS plastic with strong broad absorbance in the near-UV.

Parameter	EJ-282	EJ-286
Wavelength of maximum emission	481 nm	425 nm
Wavelength of maximum adsorbition	390 nm	355 nm
Decay time	1,9 ns	$\sim$ 1,2 ns
Quantum efficiency	93%	92%
Refrective index	1,58	

Table 3.1: Proprieties of the WLS materials used for the experiments

The absorption and emission spectra of these two WLS materials were taken from Eljen Technology website and are shown in fig. 3.1 and 3.2. Both materials are suitable to be used with incoming

UV light: in the range 350-400 nm for EJ-282 and 360-390 nm for EJ-286. The EJ-286 broader wavelength absorption range makes it particularly suitable to be used as first shifter in double-shift light trap configuration.

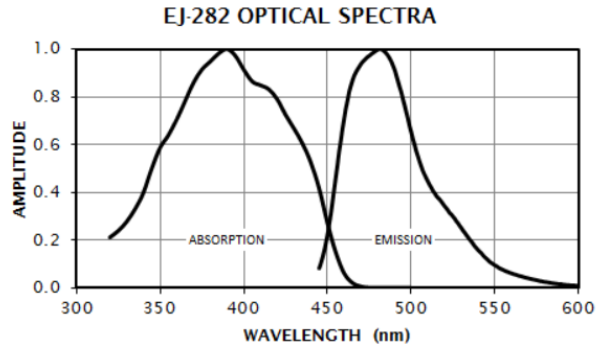

Figure 3.1: Wavelength rage for absorption and emission WLS EJ-282, [10].

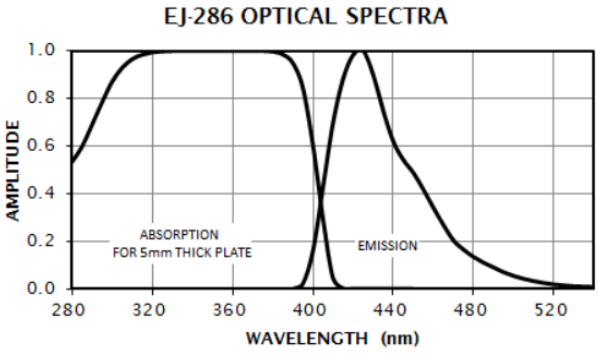

Figure 3.2: Wavelength rage for absorption and emission WLS EJ-286, [10].

The WLSs used as second shifters are optical fibres from Kuraray manufacturing. The two types selected, YS-2 and YS-6, are both blue-to-green shifters. Properties and spectra are shown in the following table 3.3 and fig. 3.2, both taken from Kuraray website.

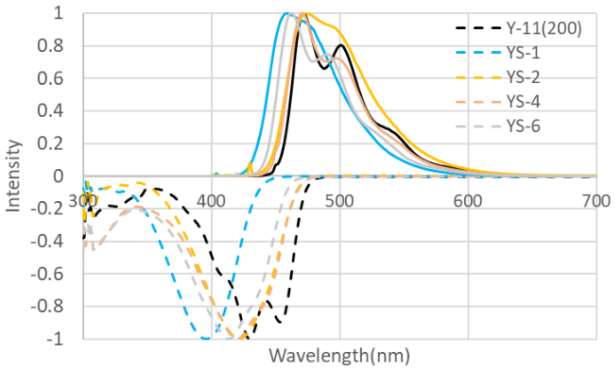

Table 3.2: Absorption and emission spectra for different types of fibers (in this case YS-2 and YS-6) [8].

Parameter	YS-2	YS-6
Absorption peak	422 nm	414 nm
Emission peak	474 nm	462 nm
Decay time	3,2 ns	1,3 ns

Table 3.3: Proprieties of the WLS Kuraray fibers used for the experiments

The laser generator used in our measures provides an UV emission at $\sim$ 375nm and, at this wavelength, EJ-282 and EJ-286 have an almost total UV absorption capacity (fig. 3.1 and fig. 3.2).
Since EJ-282 is shifting light in a close vicinity of the green band, this WLS can be actually used in single-shift configuration light traps. EJ-286 is instead shifting light into the blue band and is therefore suitable to be used as first shifter in double-shift configurations. In this way, EJ-286 can be effectively coupled with both YS-2 or YS-6 which, show the maximum absorption capacity respectively at 422 and 414 nm, i.e. at wavelengths close to the maximum emission of EJ-286.

3.1.1 Physical process of light trapping

The physical process of light trapping takes advantage of the shifted photons isotropic diffusion within the material. As soon as the incoming light enters the WLS surface through an "entrance window", it is absorbed and then isotropically re-emitted at longer wavelength by the material molecules. The ability to keep the light internally the WLS can be measured by the so called

"trapping efficiency" that is a characteristic depending on the optical features of the WLS itself and the surrounding medium.

Considering a simple 2D case of a WLS shaped in two parallel flat surfaces, where n_e and n_i are the refraction indexes respectively of the external medium and the WLS material, the concept of light trapping requires that the emitted shifted photons remain trapped within the surfaces as much as possible.

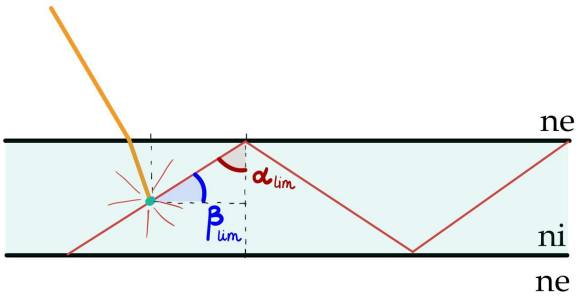

Figure 3.3: Light trapping, remission process: n_i and n_e are the refractive indexes respectively of the WLS and the external medium.

By indicating with α the incidence angle of the emitted photon in relation to the surface normal, according to Snell's law, the internal reflection is total when α equals the critical angle:

$$\alpha_{lim} = arcsin\left(\frac{n_e}{n_i}\right) \qquad \beta_{lim} = \frac{\pi}{2} - \alpha_{lim} \tag{3.1}$$

Therefore, when $\alpha > \alpha_{lim}$ or $\beta < \beta_{lim}$ the photon can escape from the lateral surfaces only. The share of trapped photons can be calculated as follows:

$$\%\ \text{trap.ph.} = \frac{4\beta_{lim}}{2\pi} = 1 - \frac{\alpha_{lim}}{\pi/2} \tag{3.2}$$

In a more general 3D case, the geometry of WLS materials is more complex and therefore we need to consider solid angles of reflection. Furthermore, the fraction of trapped photons changes with the geometry of the WLS material (i.e. it is different for fibres or parallel surfaces).
The solid angle Ω of a cone with apex angle α can be expressed with the relation:

$$\Omega = 2\pi\left(1 - cos\frac{\alpha}{2}\right)$$

Let's consider now the two cases: fibres and parallel planes.

A fibre is a long and thin tube, i.e. geometrically a cylinder. In this case the total reflection of the emitted photon occurs when the solid angle Ω equals the limit corresponding to the apex angle $2\beta_{lim}$ beyond which, the emitted photon can escape only from the two opposite bases of the cylinder:

$$\Omega_{\beta_{lim}} = 2\pi\left(1 - cos(\beta_{lim})\right)$$

The fraction of the trapped photons is:

$$\%\ \text{trap.ph.}_{fiber} = \frac{2\Omega_{\beta_{lim}}}{4\pi} = 1 - cos(\beta_{lim}) = 1 - cos\left(\frac{\pi}{2} - \alpha_{lim}\right) = 1 - sin\left(arcsin\frac{n_e}{n_i}\right)$$

$$\%\ \text{trap.ph.}_{fiber} = 1 - \frac{n_e}{n_i} \tag{3.3}$$

Considering now the case of a 3D solid WLS shaped with parallel plane surfaces, the emitted photon will escape from the lateral borders when the solid angle Ω equals the limit apex angle $2\alpha_{lim}$:

$$\Omega_{\alpha_{lim}} = 2\pi\,(1 - cos(\alpha_{lim})) \quad \Rightarrow \quad 2\Omega_{\beta_{lim}} = 4\pi - 2\Omega_{\alpha_{lim}} = 4\pi cos(\alpha_{lim})$$

The fraction of the trapped photons is:

$$\%\ \text{trap.ph.}_{planes} = \frac{2\Omega_{\beta_{lim}}}{4\pi} = cos(\alpha_{lim}) = cos\left(arcsin\frac{n_e}{n_i}\right)$$

$$\%\ \text{trap.ph.}_{planes} = \sqrt{1 - \left(\frac{n_e}{n_i}\right)^2} \tag{3.4}$$

In conclusion, for a given geometry, the relevant trapping efficiency can be calculated as a function of the refractive indexes. EJ-282 and EJ-286 panels have a refractive index of about n_i =1,58. For the fibre cores the refractive index is about n_i =1,59. Commonly, air ($n_e = 1$) or water (n_e = 1,33) are used as external media and with the WLS material considered we have:

- **Trapping efficiency for fibres**:
  in air ($n_e = 1$) % trap.ph.$_A \sim 37\%$, in water ($n_e = 1,33$) % trap.ph.$_W \sim 16\%$;
- **Trapping efficiency for parallel surfaces**:
  in air ($n_e = 1$) % trap.ph.$_A \sim 77\%$, in water ($n_e = 1,33$) % trap.ph.$_W \sim 54\%$.

From a construction point of view, fibres are provided with a single or multi-cladding on the external cylindric surface. Actually, one or more layers of lower refractive materials are in contact with a core of higher refractive material. In the Kuraray fibres used, the core has a refractive index of 1,59. For single-cladding fibres the refractive index of the layer is 1,49. For double-cladding, the index of the inner layer is 1,49 and the index of the outer layer is 1,42. This particular fibre construction ensures that the light propagation within the claddings is negligible and therefore the light remains almost completely confined within the fibre core.

3.2 Single- and double-shift layouts

In light traps, the single-shift layout is the simplest configuration. The WLS material can be properly shaped as a disk or a square and also formed by fibres. To take advantage of the light isotropic diffusion in WLS, the SiPMs are positioned on the lateral surfaces in flat solids or on the cylinder ends in tubular fibres.

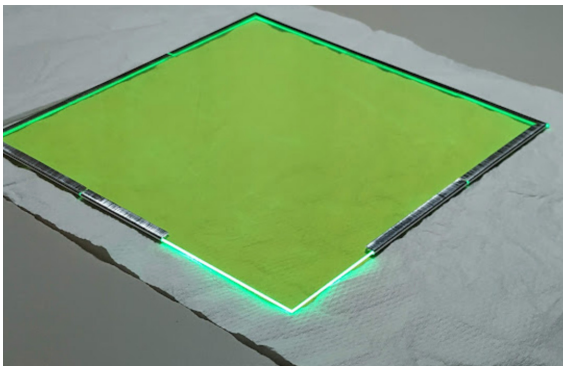

Figure 3.4: Example of single-shift layout with EJ-282 WLS

For the double-shift layout we have considered two couplings, both based on a WLS disk (EJ-286) as first shifter.

In the first configuration, the second shifter is a bundle of 7 fibres (YS-2) coiled on the disk circumferential surface. In the second one, the same disk is coiled by a bundle of 3 fibres (YS-6). In both configurations the first shift is from UV to blue and, the second one from blue to green light.

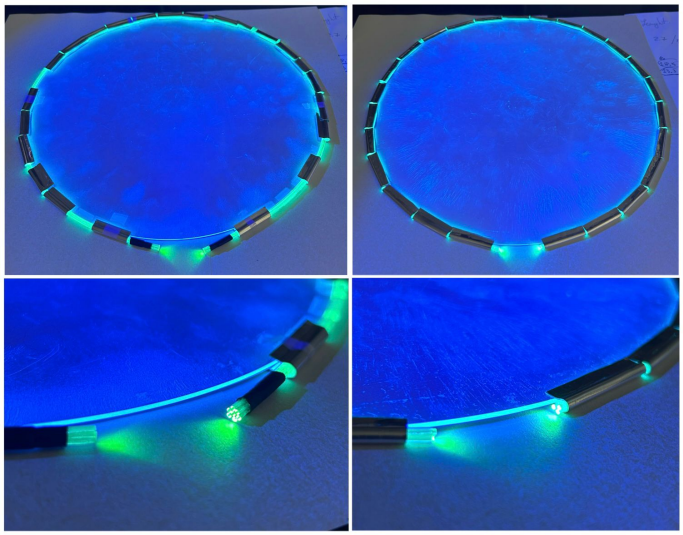

Figure 3.5: Left side: top and bottom figures show the double-shift layout with EJ-286 disk and seven bundled YS-2 fibers. Right side: top and bottom figures show the double-shift layout with EJ-286 disk and three bundled YS-6 fibers.

Besides keeping the light internally confined, the key function of a light trap is conveying the light to the photosensitive area as much as possible. Therefore, the most effective light collection process requires larger collection surfaces in respect to the photosensitive area, i.e. the areas where light sensors are located. In other terms, the light concentration on the photosensitive are can be realized through a kind of "geometrical compression" of the WLS surfaces.

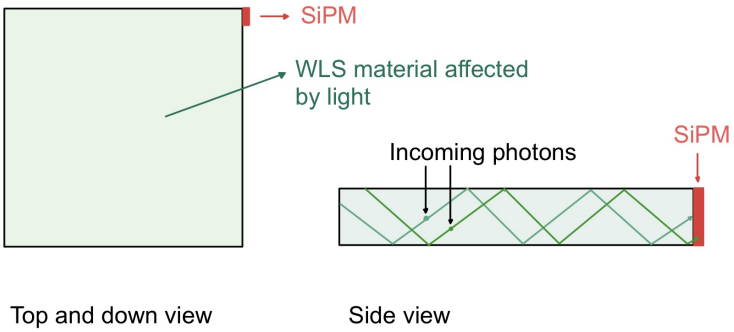

Figure 3.6: Scheme of WLS light trapping to transport light to scintillator to the sensors. This scheme explain the compression of the optic surface for single-shift.

As an example, in a single-shift layout, if the total area of the square plate collecting the light is S_{tot} = 15x15 cm^2 = 225 cm^2 and the lateral area is $S_{lat} = 4 \cdot 15$ cm $\cdot\, 0,1$ cm = 6 cm^2, the ratio between these surfaces is:

$$\frac{S_{tot}}{S_{lat}} \simeq 38$$

If now we consider a double-shift layout (disk and fibres), since the actual lateral surface is reduced just to the two small areas of the fibre ends, the above ratio can easily be more than 1000, even up to 10000 depending on the disk radius.

An issue with the single-shift configuration, is that shape and size of the available commercial SiPMs are not much suitable to steadily cover all the lateral surfaces of the WLS. Actually, elongated sensors would be more preferable, ideally matchstick-shaped, but they are not currently available due to their construction complexity and to the lack of market demand. As a result, for improving the photon flux detection, all lateral surfaces are covered with thin mirrors and the SiPMs is placed on a corner of the WLS plate (Fig. 3.7):

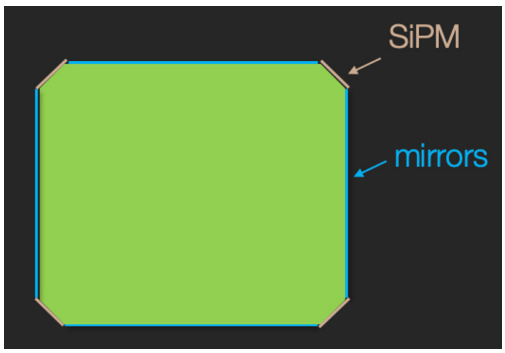

Figure 3.7: Scheme of smart WLS light trap.

As a result, the double-shift configuration is simpler for the technical implementation and also from an operational point of view. Actually, the use of a fibre bundle arranged on the circumferential surface of a primary disk-shaped WLS, allows to collect and convey all the light towards the two ends of the fibres, where it is easier to position the available light sensors.

3.3 Effects of the WLS on the pulse shape

We should reasonably expect that the interposition of WLS layers between the light source and the detection sensor may modify the original light pulse in shape and time displacement. Therefore, a larger time integration gate would provide a better temporal resolution, while a shorter integration gate would result in better SNR.
By comparing the shifted waveforms with the original laser pulse shape, in both single and double-shift configurations, we can deduct a sort of "temporal performance" of the light trap. To this purpose, we can identify three characteristic parameters of the waveform that enable analysing the changes as function of time:

- **Rise time**: it represents the duration of rising edge from 10% to 90% of the signal waveform;
- **Fall time**: it represents the duration of falling edge from 90% to 10% of the signal waveform;
- **Width (FWHM)**: it represents the full width at half maximum measured at the 50% level of the signal waveform from the positive slope.

The following figures show how rise and fall times are calculated directly from the oscilloscope.

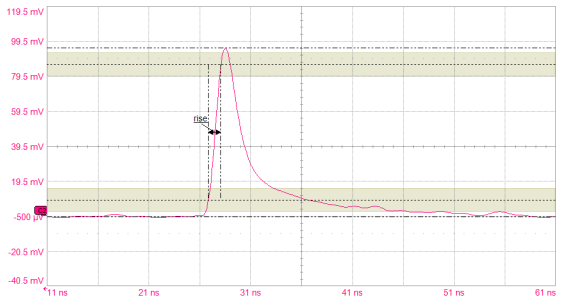

Figure 3.8: Rise time of waveform

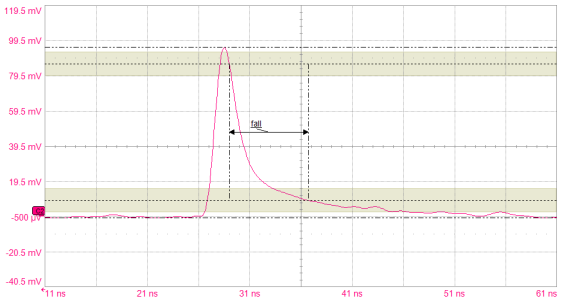

Figure 3.9: Fall time of waveform

These figures show the typical signal of incident light directly on the SiPM. When hitting the WLS molecules, the light is delayed because of the material decay time. Therefore, the shifted waveform processed by the SiPM is different from that one of the direct laser light.

In order to calculate the above mentioned parameters with statistical significance, it is advisable to consider a pulse waveform obtained as average of many single waveforms. As an example, pictures 3.10 and 3.11 show two random single waveforms detected out of the WLS, while figure 3.12 is the final average signal waveform as obtained from 1000 sweeps.

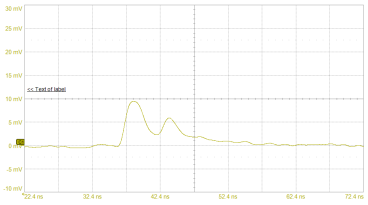

Figure 3.10

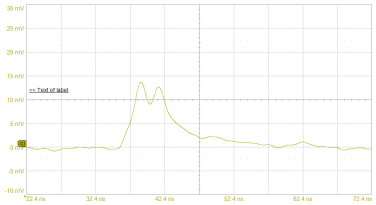

Figure 3.11

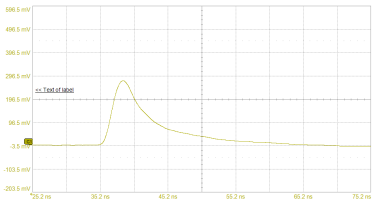

Figure 3.12

The following figures 3.13 and 3.14, show the average waveforms obtained by using different WLS materials, respectively in single and double-shift configurations. Tables 3.4 and 3.5 summarize the average values obtained for Rise time, Fall time and Width, yet in the two configurations. The average waveforms have been obtained out of 1000 sweeps.

For the single-shift setup we can note that, excluding the fibre YS-2, Width is within the range of 4-6 ns. The larger Width of YS-2 may be due to the longer decay time of this material.
For the double-shift layout, the waveform width with YS-6 is less than 10 ns and slightly less than YS-2. Rise and Fall times are comparable for both materials.

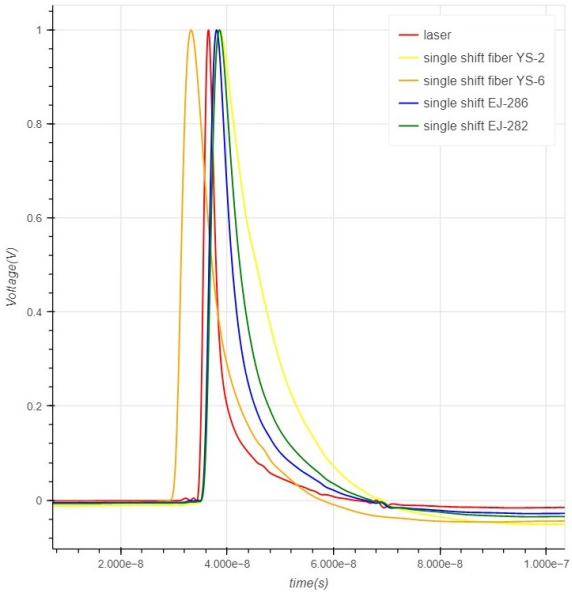

Figure 3.13: Pulse shape of single shift layout compared with the signal shape.

	rise time(ns)	fall time(ns)	width(ns)
direct	1,20	8,27	**2,43**
YS-2	1,91	21,3	**9,41**
YS-6	1,95	16,0	**6,00**
EJ-286	1,58	15,7	**4,48**
EJ-282	1,79	16,5	**5,76**

Table 3.4: Values of rising time, falling time and width for single-shift.

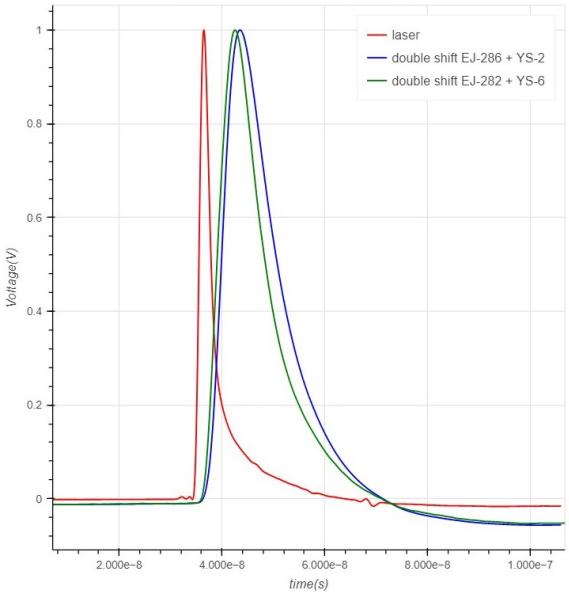

Figure 3.14: Pulse shape of double shift layout compared with the signal shape.

	rise time(ns)	fall time(ns)	width(ns)
direct	1,20	8,27	**2,43**
YS-2	4,11	19,5	**11,3**
YS-6	4,19	18,5	**9,82**

Table 3.5: Values of rising time, falling time and width. The YS-2 and YS-6 represents the fibers combining them with the disk EJ-286 to compose the double-shift layout.

The data acquired clearly show that the original light pulse is quite significantly modified by the WLS materials both in shape and temporal displacement. This result can be explained by considering the degradation of the temporal resolution induced by the WLS, which is even more evident in the double-shift layout.

Chapter 4

Considerations on light traps efficiency

In the previous section, the main features of WLS light traps were examined both in single and double-shift layouts and we gave some indications on the WLS material effects on the pulse waveform changes.
As with any other measuring device, another important consideration concerns the efficiency of the light trap, understood and seen as a single system. This is a key feature to evaluate the actual performance of the light collection process.

In general, the "Efficiency" of a light trap is just the comparison between the input and output light signals and therefore, can be defined as ratio between the number of incident photons on the WLS surface ($\#ph_{\text{incident}}$) and the number of photoelectrons produced by the SiPM ($\#phe_{\text{observed}}$), i.e. the photoelectrons actually generating the electric signal to be processed.

By recalling the expression of the SiPM Photo Detection Efficiency (1.1), the total light trap efficiency can be expressed as:

$$\epsilon = \frac{\#ph_{\text{observed}}}{\#phe_{\text{incident}}} = \frac{1}{PDE} \cdot \frac{\#phe_{\text{observed}}}{\#phe_{\text{incident}}} \tag{4.1}$$

An in-deep study of the efficiency is depending on multiple influencing factors and therefore it is out of the scope of this thesis work. For this reason, we will just stay on making a general assessment based on some assumptions, applied just to double-shift light traps.

4.1 Laser stability during time

As an important starting point, the laser light intensity should be stable over the time or, at least, continuously monitored with a second sensor, because the laser instability would reflect both on the number of incident photoelectrons and the SiPM Gain. Since the measurements of incoming and shifted lights are taken in sequence and not at the same time, we have to expect changes of Gain and number of photoelectrons during the time.

By setting the laser to emit a significant flux of about 100 photons, we took repeated measures of the average number of photoelectrons and then calculated Gain with the corrected formula 2.5:

$$G = \frac{\bar{A} - \bar{A}_{ped}}{\mu}$$

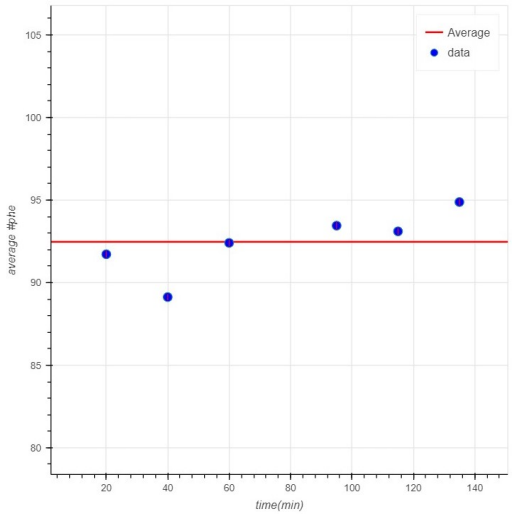

Figure 4.1: Pattern of the average number of photoelectrons μ during time

time (min)	$\mu \pm \sigma_\mu$
20	91,72± 0,20
40	89,12± 0,18
60	92,40± 0,21
95	93,45± 0,21
115	93,10± 0,21
135	94,88± 0,20

Table 4.1: μ represents the average number of photoelectrons and σ_μ is its error

From the data collected we can note that the average number of photoelectrons μ is varying within a 10% range. From the data of tab. 4.1 we have an average number of incident photoelectrons:

$$\bar{\mu} = 92.4 \pm 1.8$$

In the same way we can proceed with repeated measures of the Gain:

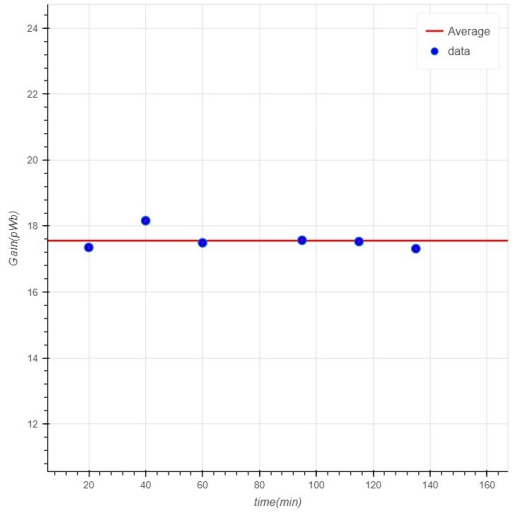

Figure 4.2: Pattern of the Gain (G) during time

time (min)	$G \pm \sigma_G$ (pWb)
20	17,35± 0,05
40	18,16± 0,05
60	17,49± 0,05
95	17,57± 0,05
115	17,53± 0,05
135	17,31± 0,04

Table 4.2: G represents the gain and σ_G is the associated error

Also for the Gain the changes during the time are within a 10% range and the average of the measures is:

$$G = (17.57 \pm 0.28)\ pWb$$

In conclusion, despite a fixed setting of the laser, the measurements show substantial changes and therefore we can conclude that the actual laser intensity instability induces a systematic error of 10%.

4.2 Efficiency influencing factors

In a double-shift light trap in air, the efficiency depends on several kind of losses coming from the different coupled components:

- Disk absorption efficiency: ∼100% (sec. 3.1);
- Disk re-emission efficiency (loss of incident photons): ∼92% for the EJ-286 (material data sheet);
- Disk trapping efficiency: in air ∼77% (sec. 3.1.1);
- Fiber trapping efficiency: in air ∼37% (sec. 3.1.1);
- Losses through re-absorption inside the tile and at the transition between disk and fiber (small because attenuation length much larger than the dimensions of the disk);
- Absorption efficiency of fiber: depends on the number of fibers in a bundle and the overlap of the disk emission and the fiber absorption spectra;
- Fiber re-emission efficiency: ∼90% (material data sheet);
- Losses due to re-absorption inside the fiber and at the transition between fiber and SiPM.

Some of these losses are unknown or can be just assessed in a qualitative way. Besides this, we have to consider the presence of the systematic error caused by the laser instability. Finally, another possible systematic error to be added to the previous factors is caused by the mismatch of the fiber emission spectrum and the PDE of the SiPM.

4.3 Efficiency measurements

For our experiment we have considered two double-shift experimental light traps as seen in sec. 3.2 (external medium: air): one formed by an EJ-286 disk fitted with a bundle of 7 YS-2 fibers and the other one by the same disk with a bundle of 3 YS-6 fibers.

4.3.1 Expected result of light detection efficiency

In a recent article [6] the efficiency of similar double-shift light traps was theoretically calculated by considering all known influencing factors and the result was reported to be in the range of 17%-20% in air. On the contrary, the actual measured value by the Authors resulted to be around 3%.

Considering that the precise individuation of each effect that factorize the whole efficiency goes beyond the scope of this thesis, we expect to get a quantitative result that, although affected by a quite significant error, should result at least in line with that one obtained by the a.m. Authors.

4.3.2 Set-up of the experiment and measurements

Recalling the definition (4.1), in order to measure the efficiency of light traps, we need to calculate the number of photoelectrons that affect the WLS disk surface and the number of photoelectrons that are produced when light hits the SiPM pixels.

Ideally the two quantities of photoelectrons should be measured at the same time. The method is to take contemporary measurements of these quantities. However, since the laser is collimated and not diffused, an alternative procedure is possible. Such technique is based on two steps which are then repeated a sufficient number of times for stabilizing the measures:

- Initially for establishing the number of incident photons, the spot of the laser is directly positioned on the SiPM surface. In this way we can measure the number of the emitted photons by reasonably assuming that the light beam is "completely" absorbed by the pixels;

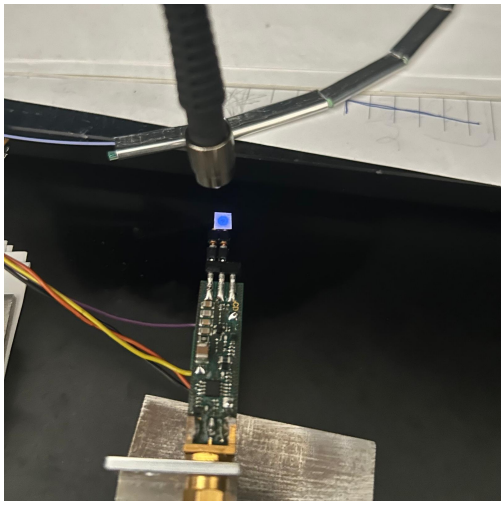

Figure 4.3: Method to measure a direct flux of photons

- As second step, by placing the laser on the centre of the WLS disk while two SiPMs are located at the ends of the fibres, then we can proceed measuring the number of photoelectrons observed by the sensors.

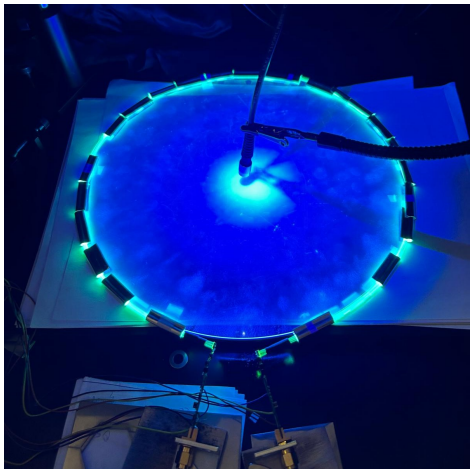

Figure 4.4: Laser spot positioned at the center of the disk

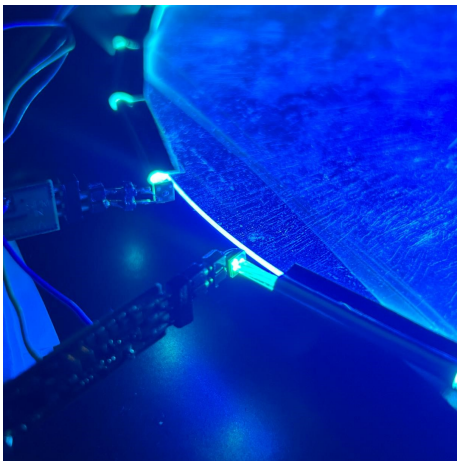

Figure 4.5: SiPMs positioned at the fibers ends

The laser is set to emit a flux of about 100 photons, in this way it's possible to see a few number of photons out the fibers.

In order to mitigate the a.m. losses, the light collecting process can be improved through the following "workarounds":

- By wrapping the fibre with a reflecting foil we get the double advantage of better supporting them around the disk and especially preventing further losses of light through the fibres;
- As additional improvement two drops of Optical Coupler (OC) were placed in between the SiPM surface and the fibre ends. The used OC is a dual component with an exceptional

refractive index (1,56) that creates a sort of meniscus improving the photon transfer to the SiPM.

	#incident photons	#photons on SiPM CH1	#photons on SiPM CH2	ϵ_{rel}
YS-6	110,25	1,59	1,55	2,85%
YS-2	87,16	1,03	0,98	2,31%

Table 4.3: Results of the relative maximum efficiency, where YS-6 represents the double-shift layout with boundle of 3 fibers and YS-2 the double-shift layout with 7 fibers.

The relative maximum efficiency ϵ_{rel} has been calculated as ratio between the average number of observed and incident photoelectrons. The full efficiency can be obtained dividing ϵ_{rel} by the value of PDE.

4.3.3 Results

As expected, the efficiency results obtained for our two configurations of double-shift layout, were not consistent with the theoretical predictions reported into the earlier mentioned article [6]. In fact, in air, the maximum efficiency achieved by the light trap fitted with the bundle of three YS-6 fibers was 2,85% while, the light trap with seven YS-2 fibers showed an efficiency slightly above 2,3%. Nevertheless, these results are in line with the 3% measured efficiency, reported in the a.m. article.

It is evident that the multiple factors influencing the efficiency have systematic and additive effects on the efficiency measurement. Therefore, from one hand, it is necessary to better understand and quantify these factors and, from the other one, possibly improve the experimental set-up and the light traps prototypes.

Regarding this last aspect, there is the suspicion that the poor efficiency of the system is caused by the fiber in which, the dopant quantity in the material does not allow a total absorption of light. This investigation will be the subject of future laboratory studies.

Chapter 5

Conclusion

In this thesis work, we have demonstrated the feasibility of effective light traps for the detection of unfocused photon fluxes using large Wavelength Shifter (WLS) collecting windows and small solid-state silicon sensors. Since optimized sensors for WLS single-shift traps (i.e. long and thin, ideally like a matchstick) are not yet available, the study and the measurements just focused on the double-shift configuration: a first large WLS plate collects UV light and transforms it into blue, and a second WLS fiber bundle collects the blue light providing a further shift in the green. In this configuration, the large geometrical compression enables achieving a considerable yield (> 1000), compared to the direct observation of light with an isolated silicon sensor, even though the overall efficiency of the system is still rather low.

This new type of photodetectors can be used in many experiments and detectors that exploit Cherenkov radiation as the main investigative tool for the reconstruction of physical events.

Key points:

- The thesis demonstrates a new method for effective light trapping in photon flux detection.
- The method uses large WLS collecting windows and small silicon sensors.
- The "double shift" configuration provides a significant yield in sensitivity.
- The new photodetector can be used in a variety of experiments and detectors.

References

[1] Renker D, Lorenz E. Advances in solid state photon detectors. JINST. 2009; 4: P04004.

[2] Kobayashi Y, Okumura A, Cassol F, Katagiri H, Sitarek J, Gliwny P, Nozaki S, Nogami Y. Camera Calibration of the CTA-LST prototype. PoS. 2021; ICRC 2021.

[3] Huentemeyer P, et al. The Southern Wide-Field Gamma-Ray Observatory (SWGO): A Next-Generation Ground-Based Survey Instrument for VHE Gamma-Ray Astronomy. Astra2020 APC White Paper. 2019.

[4] Schulte L, Vogel M, Hoffmann A, Böser S, Köpke L, Kowalski M. A large-area single photon sensor employing wavelength-shifting and light-guiding technology. ICRC 2013.

[5] Bouvier A, Gebremedhin L, Johnson C, Kuznetsov A, Williams DA, Otte N, Strausbaugh R, Hidaka N, Tajima H, Hinton J, White R, Errando M, Mukherjee R. Photosensor Characterization for the Cherenkov Telescope Array: Silicon Photomultiplier versus Multi-Anode Photomultiplier Tube. arXiv. 2013.

[6] Pihet M, Mariotti M, Arcaro C. Wavelength-shifting light traps for SWGO and other applications. PoS. 2023.

[7] Kuraray Co., Ltd. Plastic Scintillating Fibers. Kuraray Co., Ltd. 2014.

[8] Imamiya Y. Introduction of Kuraray New Short Decaytime WLSF YS-4-6. Kuraray Co., Ltd. 2022.

[9] Hamamatsu Photonics K.K. S14160/S14161 series: Low breakdown voltage type MPPC for scintillation detector. Hamamatsu Photonics K.K. 2020.

[10] Eljen Technology. Wavelength Shifting Plastics EJ-280, EJ-282, EJ-284, EJ-286. Eljen Technology. 2021.

[11] Hamamatsu Photonics. Physics and Operation of the MPPC Silicon Photomultiplier.

[12] Hamamatsu Photonics. What is an SiPM and How Does it Work?

[13] Wikipedia. Photomultiplier Tube.